Chemical Science

Accepted Manuscript

This article can be cited before page numbers have been issued, to do this please use: Y. Shao, J. Zhan, J. Deng, X. Zhang, H. Qin, J. Liu, M. Li and R. Cao, *Chem. Sci.*, 2025, DOI: 10.1039/D5SC00102A.

ROYAL SOCIETY OF CHEMISTRY

rsc.li/chemical-science

View Article Online
DOI: 10.1039/D5SC00102A

EDGE ARTICLE

In situ uncovering the catalytic cycle of electrochemical and chemical oxygen reduction mediated by iron porphyrin

Received 00th January 20xx,
Accepted 00th January 20xx

DOI: 10.1039/x0xx00000x

Xianhao Zhang,‡[ac] Jirui Zhan,‡[a] Haonan Qin,‡[b] Jintao Deng,[a] Junjie Liu,[a] Meixian Li,[a] Rui Cao*[b] and Yuanhua Shao*[a]

As one of the critical reactions in biotransformation and energy conversion processes, the oxygen reduction reaction (ORR) catalyzed by iron porphyrins has been widely explored by electrochemical, spectroscopic, and theoretical methods. However, experimental identification of all proposed intermediates of iron porphyrins in one catalytic cycle is rather challenging in the mechanistic studies of ORR driven by electrochemical or chemical methods. Herein, we report the application of electrochemical mass spectrometry (EC-MS) and chemical reaction mass spectrometry (CR-MS) to in situ uncover the catalytic cycle of electrochemical and chemical ORR mediated by an iron porphyrin molecular catalyst. Five crucial iron-oxygen intermediates detected by both EC-MS and CR-MS help to build the whole catalytic cycle and indicate the details of the $4e^-/4H^+$ pathway to produce H_2O in electrochemical and chemical ORR. By combining in situ MS methods with electrochemical and spectroscopic methods to characterize the intermediates and study the selectivities, this work provides a mechanistic comparison of electrochemical and chemical ORR catalyzed by one model iron porphyrin.

Introduction

Oxygen (O_2) reduction reaction (ORR) is a critical step in biotransformation and energy conversion processes, including biological respiration,[1,2] fuel cells,[3,4] metal-air batteries,[5,6] etc. Inspired by the heme active sites in natural cytochrome *c* oxidases,[2] iron porphyrins have been widely used and studied as molecular catalysts for ORR.[7-26] This simplified model reaction helps researchers to better understand the mechanisms and structure-activity relationships of ORR under controlled conditions with different catalyst ligands, solvents, and proton/electron sources. Depending on electron sources, ORR catalyzed by molecular complexes can be driven by electrodes or chemical reductants such as ferrocene derivatives.[21,27] Accordingly, most of the previous in situ characterization studies in this field investigated the kinetics and mechanisms of ORR by electrochemical, spectroscopic, and microscopy methods assisted with theoretical calculations.[19,28-46] Furthermore, the evidence of a series of reactive iron-oxygen intermediates has also been obtained through spectroscopic methods in single-turnover experiments mainly under extremely low temperatures (Table S1 in the ESI†).[47-52] However, the identification of all possible key intermediates proposed in one complete cycle under catalytic conditions is important but inadequate in either electrochemical or chemical ORR catalyzed by iron porphyrins,[12,18,28-31,33,43,45] which limits comprehensive comparison and understanding of the mechanistic details of ORR driven by electrochemical and chemical methods. Therefore, developing and applying novel in situ characterization methods to detect as many intermediates as possible under electrochemical and chemical conditions is urgently necessary to reveal the mechanism of ORR catalyzed by molecular complexes including iron porphyrins.

Mass spectrometry (MS) is a powerful analytical technique to characterize analytes with high sensitivity and selectivity, which is widely employed in monitoring chemical/electrochemical reactions and in elucidating their mechanisms by detecting intermediates and products.[53-58] Dual micropipettes pulled from quartz or glass theta capillaries are commonly applied as microreactors, sampling collectors, and spray emitters in MS analysis.[59-67] Utilizing hybrid ultramicroelectrodes (UMEs) fabricated from dual micropipettes, the in situ electrochemical mass spectrometry (EC-MS) developed by Shao and Luo et al. has been applied in the mechanistic studies of a series of complicated electrochemical reactions.[68-73] The in situ MS method based on dual micropipettes and hybrid UMEs would be an effective tool to identify intermediates and investigate mechanisms in both chemical and electrochemical ORR.

Herein, we apply EC-MS based on hybrid UMEs and chemical reaction mass spectrometry (CR-MS) recently developed by our group[74] to in situ reveal the mechanism of ORR mediated by a molecular catalyst 5,10,15,20-*meso*-tetraphenylporphyrin

[a] Beijing National Laboratory for Molecular Sciences, College of Chemistry and Molecular Engineering, Peking University, Beijing 100871, China. E-mail: yhshao@pku.edu.cn
[b] Key Laboratory of Applied Surface and Colloid Chemistry, Ministry of Education, School of Chemistry and Chemical Engineering, Shaanxi Normal University, Xi'an 710119, China. E-mail: ruicao@snnu.edu.cn
[c] Department of Chemistry, China Agricultural University, Beijing 100193, China.
† Electronic supplementary information (ESI) available. See DOI: 10.1039/x0xx00000x
‡ These authors have contributed equally.

View Article Online
DOI: 10.1039/D5SC01038A

iron(III) perchlorate ([(TPP)Fe^{III}]ClO_4) (Scheme 1). Five key suggested intermediates involved in electrochemical/chemical ORR were simultaneously detected for the first time by both in situ MS methods, providing full experimental evidence and mechanistic details to build the whole catalytic cycle of ORR mediated by [(TPP)Fe^{III}]$^+$.[29,31,33] Assisted with electrochemical and spectroscopic methods to determine the selectivity, the same five iron-oxygen intermediates ([(TPP)Fe^{III}–$O_2^{\bullet-}$], [(TPP)Fe^{III}–$O_2^{\bullet}$H]$^+$, [(TPP)Fe^{III}–O_2H_2]$^+$, [(TPP)Fe^{V}=O]$^+$, and [(TPP)Fe^{IV}–OH]$^+$) detected with exact chemical compositional information by both EC-MS and CR-MS suggest a good agreement of a $4e^-/4H^+$ mechanism in electrochemical and chemical ORR catalyzed by [(TPP)Fe^{III}]$^+$. This work provides a methodology containing two sets of complementary methods to characterize the intermediates and study the mechanisms of electrochemical/chemical redox reactions mediated by molecular catalysts, including ORR catalyzed by iron porphyrins.

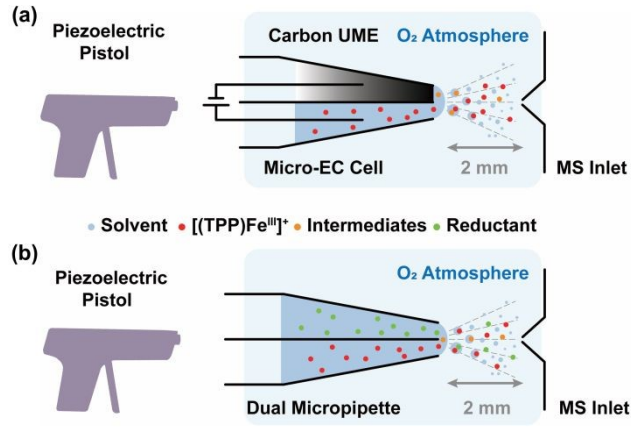

Scheme 1 Schematic illustration of the in situ MS setups to study (a) electrochemical and (b) chemical ORR mediated by [(TPP)Fe^{III}]$^+$.

Results and discussion

Electrochemical ORR

Electrochemical ORR mediated by [(TPP)Fe^{III}]$^+$ was studied by voltammetry and in situ EC-MS. The electrochemical behaviors of [(TPP)Fe^{III}]ClO_4 as an ORR molecular catalyst were first investigated on the carbon hybrid UME in *N*,*N*-dimethylformamide (DMF) with excess perchloric acid ($HClO_4$) as the proton source in the absence and presence of O_2 (Cell 1 in the ESI). The carbon hybrid UME was fabricated from quartz dual micropipettes according to the reported procedures (Fig. S1†).[73,75] In the cyclic voltammetry (CV) results (Fig. 1), black (1 atm N_2) and red (1 atm O_2) curves show the potential windows of the carbon UME using Cell 1 without [(TPP)Fe^{III}]ClO_4. When [(TPP)Fe^{III}]ClO_4 was added under 1 atm N_2, a new reversible steady-state curve (blue) emerged, which ascribing to the reduction of [(TPP)Fe^{III}]$^+$ to [(TPP)Fe^{II}] (the half-wave potential $E_{1/2}$ = −0.55 V vs. Fc^+/Fc). When [(TPP)Fe^{III}]ClO_4 was added under 1 atm O_2, the CV curve (green) showed much higher currents than that in the presence of [(TPP)Fe^{III}]$^+$ and N_2 (blue), indicating the occurrence of catalytic ORR. The electrochemical ORR mediated by [(TPP)Fe^{III}]$^+$ on the carbon UME is comparable to those observed on the glassy carbon (GC) electrode in previous reports,[29,41] which proves that the redox state of [(TPP)Fe^{III}]$^+$ can be controlled to catalyze ORR by applying the potential on the carbon UME under steady-state conditions. Furthermore, the selectivity of electrochemical ORR mediated by [(TPP)Fe^{III}]ClO_4 was also studied by rotating ring-disk voltammetry (RRDV) under the same conditions (Cell 2 in the ESI). The results of RRDV provide that the catalytic ORR (GC disk current) occurred and a trace of H_2O_2 (Pt ring current) was generated simultaneously when the voltage was less than −0.55 V vs. Fc^+/Fc (Fig. S2†). The average number of electrons n_{cat} transferred in electrochemical ORR equals $3.88e^-/O_2$ from −0.6 V to −0.9 V vs. Fc^+/Fc (Table S2†). The selectivity studies by RRDV confirmed that the $4e^-/4H^+$ pathway is dominant in electrochemical ORR catalyzed by [(TPP)Fe^{III}]ClO_4.

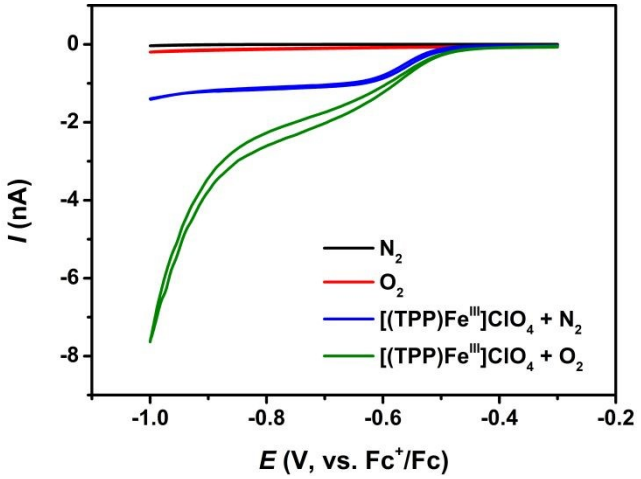

Fig. 1 CV curves of 0.5 mM [(TPP)Fe^{III}]ClO_4 in the absence (blue) and presence (green) of 1 atm O_2 on a carbon UME in DMF (Cell 1). Black (with N_2) and red (with O_2) curves are the potential windows of the carbon UME using Cell 1 without [(TPP)Fe^{III}]ClO_4.

Based on the above results by electrochemical characterization of ORR mediated by [(TPP)Fe^{III}]ClO_4, in situ EC-MS experiments were performed with Cell 3 (in the ESI) under 1 atm O_2 using the oxygenated EC-MS setup which combines hybrid UME techniques and relay electrospray ionization MS (Scheme 1a and Fig. S3†).[68,76] When the voltage of carbon UME was off, only [(TPP)Fe^{III}]$^+$ (*m/z* 668), [(TPP)Fe^{III}–DMF]$^+$ (*m/z* 741), and background signals were detected (Fig. S4†). When the voltage was on (at −0.6 V to −0.9 V vs. Fc^+/Fc), five new signals, *m/z* 684, *m/z* 685, *m/z* 700, *m/z* 701, and *m/z* 702, could be simultaneously detected by MS along with the catalyst signal (Fig. 2 and Fig. S5†). The signals of *m/z* 700, *m/z* 701, and *m/z* 702 differed by *m/z* 1 probably correspond to the intermediate [(TPP)Fe^{III}–O_2]$^+$ (ionized from [(TPP)Fe^{III}–$O_2^{\bullet-}$] by the principle of relay electrospray ionization),[76] [(TPP)Fe^{III}–$O_2^{\bullet}$H]$^+$, and [(TPP)Fe^{III}–O_2H_2]$^+$, respectively. According to the relative abundance, the signal of *m/z* 701 and the signal of *m/z* 702 may contain the isotope peak of [(TPP)Fe^{III}–O_2]$^+$ and

$[(TPP)Fe^{III}–O_2{}^{\bullet}H]^+$, respectively. Likewise, the signal of *m/z* 685 might also correspond to a mixture including the monoisotopic mass peak of $[(TPP)Fe^{IV}–OH]^+$ and the isotope peak of $[(TPP)Fe^{V}=O]^+$. The iron-oxo species could also be $[(TPP^{\bullet})Fe^{IV}=O]^+$ form[77] and we uniformly represented it in the formal $[(TPP)Fe^{V}=O]^+$ form in this work. The crucial intermediates $[(TPP)Fe^{V}=O]^+$ and $[(TPP)Fe^{IV}–OH]^+$ detected by EC-MS indicate that electrochemical ORR catalyzed by $[(TPP)Fe^{III}]^+$ involves a $4e^-/4H^+$ pathway to produce H_2O under described conditions.

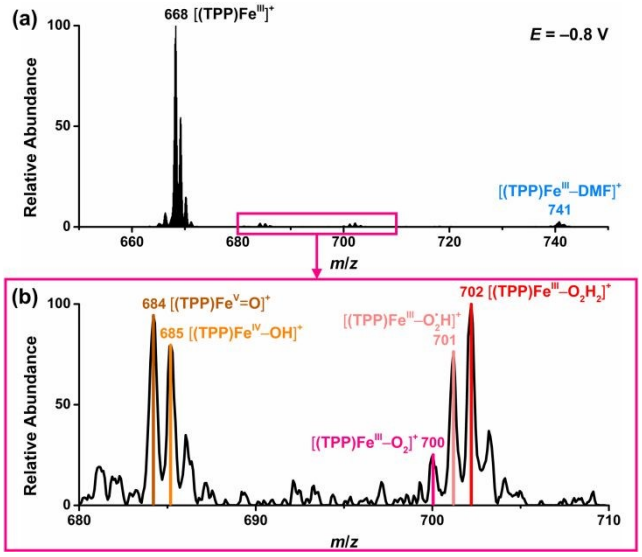

Fig. 2 Mass spectra of electrochemical ORR catalyzed by $[(TPP)Fe^{III}]^+$ in DMF when the voltage was at −0.8 V vs. Fc^+/Fc.

Chemical ORR

For chemical ORR mediated by $[(TPP)Fe^{III}]^+$, stopped-flow UV-vis spectroscopy was first used to detect the intermediates and study the selectivity. The experiments were performed by mixing a solution of air-saturated DMF containing 0.05 mM $[(TPP)Fe^{III}]ClO_4$ and 5 mM $HClO_4$ with an equal volume of an air-saturated DMF solution of 5 mM decamethylferrocene ($Me_{10}Fc$) in a stopped-flow instrument.[41] Fig. 3a shows that the signals of iron porphyrin intermediates gradually changed with the increasing concentration of $Me_{10}Fc^+$ (715 nm), suggesting the occurrence of the catalytic ORR. By comparing the results with known spectra of iron porphyrins,[78] the intermediate of Fe^{II} can be identified, while the spectra of other intermediates are overlapped and cannot be distinguished. The selectivity of chemical ORR catalyzed by $[(TPP)Fe^{III}]ClO_4$ was indicated by determining the amount of $Me_{10}Fc^+$ produced in ORR. The results in Fig. 3b suggest that the n_{cat} consumed in chemical ORR equals $3.90e^-/O_2$, which is close to that in electrochemical ORR.

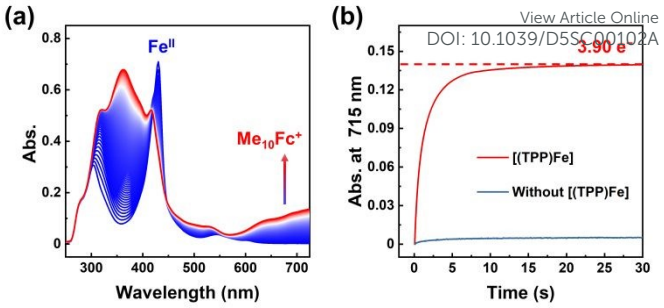

Fig. 3 (a) UV-vis spectra observed during chemical ORR with $[(TPP)Fe^{III}]ClO_4$. (b) Time profiles of the $Me_{10}Fc^+$ formation during chemical ORR with and without $[(TPP)Fe^{III}]ClO_4$.

To further investigate the mechanism of chemical ORR catalyzed by $[(TPP)Fe^{III}]^+$ in DMF, in situ CR-MS experiments were performed with 10 mM $Me_{10}Fc$ and 1 mM $[(TPP)Fe^{III}]ClO_4$ separately in each barrel of a quartz dual micropipette reactor under 1 atm O_2 using the same oxygenated MS setup (Scheme 1b and Fig. S3†). $HClO_4$ (5 mM) and $[Bu_4N][PF_6]$ (10 mM) were added in both barrels of the dual micropipette. Fig. S6† shows that only $[(TPP)Fe^{III}]^+$ (*m/z* 668), $[(TPP)Fe^{III}–DMF]^+$ (*m/z* 741), and background signals were detected when no $Me_{10}Fc$ was added. When the reductant $Me_{10}Fc$ was added, the signals of the five intermediates, $[(TPP)Fe^{V}=O]^+$ (*m/z* 684), $[(TPP)Fe^{IV}–OH]^+$ (*m/z* 685), $[(TPP)Fe^{III}–O_2]^+$ (*m/z* 700), $[(TPP)Fe^{III}–O_2{}^{\bullet}H]^+$ (*m/z* 701), and $[(TPP)Fe^{III}–O_2H_2]^+$ (*m/z* 702) were simultaneously detected by MS (Fig. 4). The detected species of iron-oxygen intermediates in chemical ORR are the same as those in electrochemical ORR, which proves the same $4e^-/4H^+$ mechanism in ORR driven by both the electrode and the chemical reductant. Additionally, it should be pointed out that the peaks of *m/z* 686 and *m/z* 703 in both electrochemical and chemical ORR are attributed to the second strongest isotopic peaks of MS spectra for $[(TPP)Fe^{IV}–OH]^+$ and $[(TPP)Fe^{III}–O_2H_2]^+$, respectively.

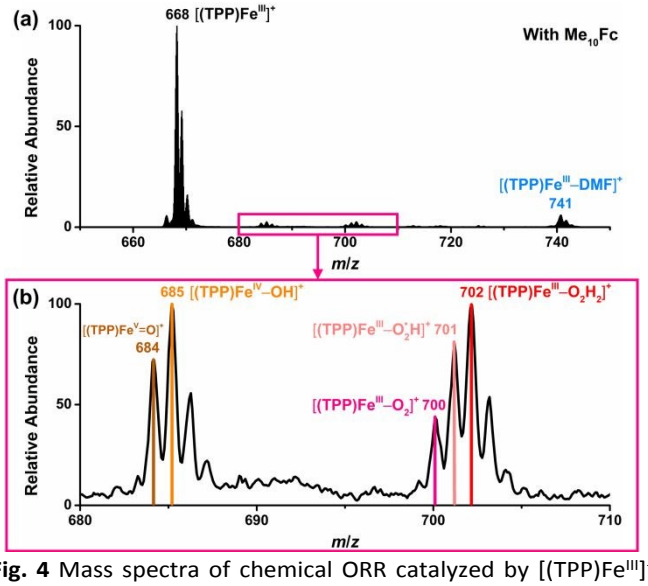

Fig. 4 Mass spectra of chemical ORR catalyzed by $[(TPP)Fe^{III}]^+$ with $Me_{10}Fc$ as the reductant in DMF.

View Article Online
DOI: 10.1039/D5SC00103A

Isotope-labeling experiments and ORR mechanism

To further confirm the iron-oxygen intermediates, isotope-labeling electrochemical and chemical ORR were performed and measured by in situ MS, using $^{18}O_2$ (97 atom% ^{18}O) in place of $^{16}O_2$ under the same conditions. As shown in Fig. 5, $[(TPP)Fe^{V}=^{18}O]^+$ (*m/z* 686), $[(TPP)Fe^{III}–^{18}O_2]^+$ (*m/z* 704), and $[(TPP)Fe^{III}–^{18}O_2H_2]^+$ (*m/z* 706) were all detected by MS in both electrochemical and chemical ORR, while $[(TPP)Fe^{IV}–^{18}OH]^+$ (*m/z* 687) can only be identified in electrochemical ORR because its signal intensity is much higher than the relative abundance of the second strongest isotopic peak of $[(TPP)Fe^{V}=^{18}O]^+$. In addition, possible $[(TPP)Fe^{III}–^{18}O_2{}^{\bullet}H]^+$ cannot be identified in the isotopic experiments due to the signal intensity of *m/z* 705 being close to that of the second strongest isotopic peak of $[(TPP)Fe^{III}–^{18}O_2]^+$.

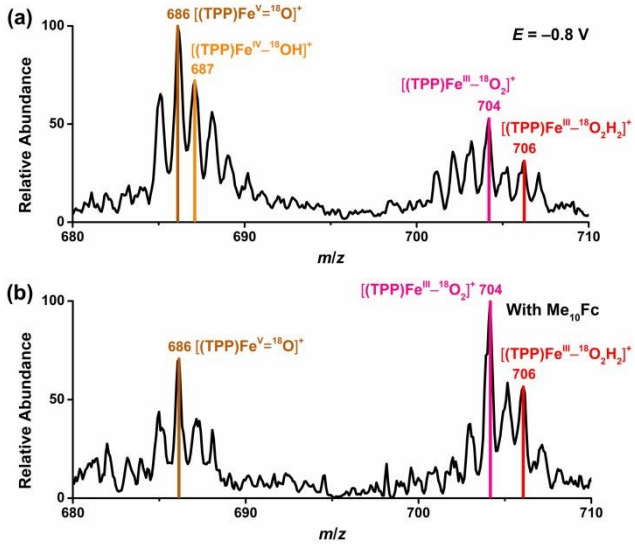

Fig. 5 Mass spectra of $^{18}O_2$-labeling (a) electrochemical and (b) chemical ORR catalyzed by $[(TPP)Fe^{III}]^+$.

According to the above in situ EC-MS/CR-MS, RRDV, and UV-vis spectroscopy results, five iron-oxygen intermediates, including $[(TPP)Fe^{III}–O_2{}^{\bullet-}]$, $[(TPP)Fe^{III}–O_2{}^{\bullet}H]^+$, $[(TPP)Fe^{III}–O_2H_2]^+$, $[(TPP)Fe^{V}=O]^+$, and $[(TPP)Fe^{IV}–OH]^+$, are experimentally confirmed to be produced in both electrochemical and chemical ORR catalyzed by $[(TPP)Fe^{III}]^+$. Scheme 2 shows the proposed mechanism of $4e^-/4H^+$ ORR based on the experimental results in this work and kinetic analysis in previous reports.[31,33,77] Note that we used formal oxidation/reduction states to assign these intermediates. In the catalytic cycle of ORR with $[(TPP)Fe^{III}]^+$ as the catalyst, $[(TPP)Fe^{III}]^+$ is first reduced by the electrode or $Me_{10}Fc$ to give $[(TPP)Fe^{II}]$. After that, $[(TPP)Fe^{II}]$ binds an O_2 molecule to produce the ferric superoxide $[(TPP)Fe^{III}–O_2{}^{\bullet-}]$, and then $[(TPP)Fe^{III}–O_2{}^{\bullet-}]$ is protonated to form $[(TPP)Fe^{III}–O_2{}^{\bullet}H]^+$.[31,33] The perhydroxyl complex $[(TPP)Fe^{III}–O_2{}^{\bullet}H]^+$ is next protonated at the distal oxygen along with 1 eq. electron (proton-coupled electron transfer, PCET) to form $[(TPP)Fe^{III}–O_2H_2]^+$ and then $[(TPP)Fe^{III}–O_2H_2]^+$ releases 1 eq. H_2O to produce $[(TPP)Fe^{V}=O]^+$.[12,20] Subsequently, $[(TPP)Fe^{V}=O]^+$ undergoes successive PCET processes to produce $[(TPP)Fe^{IV}–OH]^+$ and $[(TPP)Fe^{III}]^+$ along with 1 eq. H_2O to finally restart the catalytic cycle of ORR.[77] Among these intermediates, $[(TPP)Fe^{III}–O_2H_2]^+$ is the key to determining the selectivity of ORR catalyzed by $[(TPP)Fe^{III}]^+$ and its exact configuration has two possible forms ($[(TPP)Fe^{III}–OOH_2]^+$ and $[(TPP)Fe^{III}–HOOH]^+$).[12] In the $4e^-/4H^+$ pathway, the water could be produced via the $[(TPP)Fe^{III}–OOH_2]^+$ configuration. For ORR catalyzed by $[(TPP)Fe^{III}]^+$, the main difference between electrochemical and chemical-driven methods is the resource of electrons, one is from the electrode, and the other is from the reductant. The consistent results of mechanism and selectivity together confirm the agreement of ORR driven by these two methods.

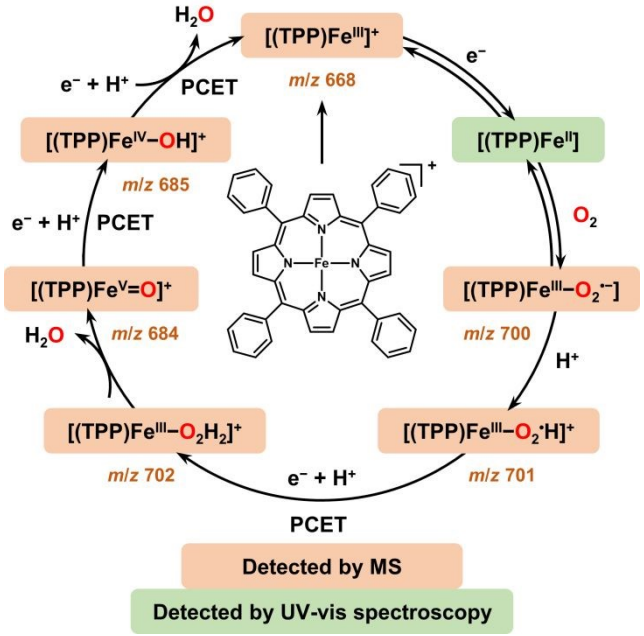

Scheme 2 Proposed mechanism of $4e^-/4H^+$ ORR with $[(TPP)Fe^{III}]^+$ as the catalyst.[12,20,31,33,77]

Conclusions

In summary, we have investigated the mechanism of electrochemical/chemical ORR catalyzed by $[(TPP)Fe^{III}]ClO_4$ using in situ EC-MS/CR-MS assisted with electrochemical characterization and stopped-flow UV-vis spectroscopy. The crucial iron-oxygen intermediates detected by in situ MS give detailed experimental evidence to establish the complete catalytic cycle of ORR with $[(TPP)Fe^{III}]^+$ as a molecular catalyst and indicate a $4e^-/4H^+$ mechanism of this reaction, further supplementing the mechanistic details lacked in previous studies.[29,31,33] This work provides a set of systematical in situ analytical methods to study the mechanisms of electrochemical and chemical redox reactions mediated by molecular catalysts. Future work needs to try more kinds of hybrid UMEs and explore the mechanisms of PCET reactions mediated by other molecular catalysts, not limited to ORR.

Data availability

All experimental data are available in the manuscript and ESI.†

Author contributions

Y. Shao and R. Cao conceived and designed the project. X. Zhang and J. Zhan developed the in situ mass spectrometry techniques. Y. Shao supervised the experiments of electrochemistry and mass spectrometry. R. Cao supervised the catalyst synthesis and the experiments of UV-vis spectroscopy. X. Zhang and J. Zhan carried out the experiments of electrochemistry and mass spectrometry. H. Qin carried out the experiments of catalyst synthesis and UV-vis spectroscopy. J. Deng assisted in the experiments of electrochemistry and mass spectrometry. All authors contributed to the discussion of the results and the preparation of the manuscript.

Conflicts of interest

The authors declare no conflict of interest.

Acknowledgements

This work was supported by the National Natural Science Foundation of China (22034001, 22304003, 22325202, and 22171176), the Beijing National Laboratory for Molecular Sciences (BNLMS-CXXM-202008), and Research Funds of Shaanxi Normal University. We thank Prof. Yan Li and Dr. Jian Sheng at Peking University for their help on RRDV experiments.

References

1. G. T. Babcock and M. Wikström, *Nature*, 1992, **356**, 301-309.
2. S. Yoshikawa and A. Shimada, *Chem. Rev.*, 2015, **115**, 1936-1989.
3. Y. Li, M.-Y. Chen, B.-A. Lu and J.-N. Zhang, *J. Electrochem.*, 2023, **29**, 2215002.
4. S. Li, L. Shi, Y. Guo, J. Wang, D. Liu and S. Zhao, *Chem. Sci.*, 2024, **15**, 11188-11228.
5. F. Cheng and J. Chen, *Chem. Soc. Rev.*, 2012, **41**, 2172-2192.
6. Y. Su, Z. Zhao, J. Huang, E. Wang and Z. Peng, *J. Phys. Chem. C*, 2022, **126**, 1243-1255.
7. M. L. Rigsby, D. J. Wasylenko, M. L. Pegis and J. M. Mayer, *J. Am. Chem. Soc.*, 2015, **137**, 4296-4299.
8. Y. Xuan, X. Huang and B. Su, *J. Phys. Chem. C*, 2015, **119**, 11685-11693.
9. X. Huang, Y. Xuan, L. Xie and B. Su, *ChemElectroChem*, 2016, **3**, 1781-1786.
10. S. Bhunia, A. Rana, P. Roy, D. J. Martin, M. L. Pegis, B. Roy and A. Dey, *J. Am. Chem. Soc.*, 2018, **140**, 9444-9457.
11. A. Ghatak, S. Bhakta, S. Bhunia and A. Dey, *Chem. Sci.*, 2019, **10**, 9692-9698.
12. A. C. Brezny, S. I. Johnson, S. Raugei and J. M. Mayer, *J. Am. Chem. Soc.*, 2020, **142**, 4108-4113.
13. A. Singha, A. Mondal, A. Nayek, S. G. Dey and A. Dey, *J. Am. Chem. Soc.*, 2020, **142**, 21810-21828.
14. A. C. Brezny, H. S. Nedzbala and J. M. Mayer, *Chem. Commun.*, 2021, **57**, 1202-1205.
15. B. D. Groff and J. M. Mayer, *ACS Catal.*, 2022, **12**, 11692-11696.
16. S. Bhunia, A. Ghatak, A. Rana and A. Dey, *J. Am. Chem. Soc.*, 2023, **145**, 3812-3825.
17. D. Nishiori, J. P. Menzel, N. Armada, E. A. Reyes Cruz, B. L. Nannenga, V. S. Batista and G. F. Moore, *J. Am. Chem. Soc.*, 2024, **146**, 11622-11633.
18. A. K. Surendran, A. Y. Pereverzev and J. Roithová, *J. Am. Chem. Soc.*, 2024, **146**, 15619-15626.
19. S. Chatterjee, K. Sengupta, B. Mondal, S. Dey and A. Dey, *Acc. Chem. Res.*, 2017, **50**, 1744-1753.
20. W. Zhang, W. Lai and R. Cao, *Chem. Rev.*, 2017, **117**, 3717-3797.
21. M. L. Pegis, C. F. Wise, D. J. Martin and J. M. Mayer, *Chem. Rev.*, 2018, **118**, 2340-2391.
22. H. Lei, X. Li, J. Meng, H. Zheng, W. Zhang and R. Cao, *ACS Catal.*, 2019, **9**, 4320-4344.
23. C. W. Machan, *ACS Catal.*, 2020, **10**, 2640-2655.
24. Y. Li, N. Wang, H. Lei, X. Li, H. Zheng, H. Wang, W. Zhang and R. Cao, *Coord. Chem. Rev.*, 2021, **442**, 213996.
25. S. Bhunia, A. Ghatak and A. Dey, *Chem. Rev.*, 2022, **122**, 12370-12426.
26. X. Li, H. Lei, L. Xie, N. Wang, W. Zhang and R. Cao, *Acc. Chem. Res.*, 2022, **55**, 878-892.
27. A. W. Nichols, E. N. Cook, Y. J. Gan, P. R. Miedaner, J. M. Dressel, D. A. Dickie, H. S. Shafaat and C. W. Machan, *J. Am. Chem. Soc.*, 2021, **143**, 13065-13073.
28. K. Sengupta, S. Chatterjee, S. Samanta and A. Dey, *Proc. Natl. Acad. Sci. U. S. A.*, 2013, **110**, 8431-8436.
29. D. J. Wasylenko, C. Rodríguez, M. L. Pegis and J. M. Mayer, *J. Am. Chem. Soc.*, 2014, **136**, 12544-12547.
30. C. Costentin, H. Dridi and J.-M. Savéant, *J. Am. Chem. Soc.*, 2015, **137**, 13535-13544.
31. M. L. Pegis, B. A. McKeown, N. Kumar, K. Lang, D. J. Wasylenko, X. P. Zhang, S. Raugei and J. M. Mayer, *ACS Cent. Sci.*, 2016, **2**, 850-856.
32. C. Costentin and J.-M. Savéant, *J. Am. Chem. Soc.*, 2018, **140**, 16669-16675.
33. M. L. Pegis, D. J. Martin, C. F. Wise, A. C. Brezny, S. I. Johnson, L. E. Johnson, N. Kumar, S. Raugei and J. M. Mayer, *J. Am. Chem. Soc.*, 2019, **141**, 8315-8326.
34. Y. Liu, G. Zhou, Z. Zhang, H. Lei, Z. Yao, J. Li, J. Lin and R. Cao, *Chem. Sci.*, 2020, **11**, 87-96.
35. A. Facchin, T. Kosmala, A. Gennaro and C. Durante, *ChemElectroChem*, 2020, **7**, 1431-1437.
36. J. Meng, H. Qin, H. Lei, X. Li, J. Fan, W. Zhang, U.-P. Apfel and R. Cao, *Angew. Chem. Int. Ed.*, 2023, **62**, e202312255.
37. J. Han, H. Tan, K. Guo, H. Lv, X. Peng, W. Zhang, H. Lin, U.-P. Apfel and R. Cao, *Angew. Chem. Int. Ed.*, 2024, **63**, e202409793.
38. T. Liu, H. Qin, Y. Xu, X. Peng, W. Zhang and R. Cao, *ACS Catal.*, 2024, **14**, 6644-6649.
39. A. Facchin, D. Forrer, M. Zerbetto, F. Cazzadori, A. Vittadini and C. Durante, *ACS Catal.*, 2024, **14**, 14373-14386.
40. A. Santra, A. Das, S. Kaur, P. Jain, P. P. Ingole and S. Paria, *Chem. Sci.*, 2024, **15**, 4095-4105.
41. H. Qin, J. Kong, X. Peng, Z. Wang, X. Li, H. Lei, W. Zhang and R. Cao, *ChemSusChem*, 2025, **18**, e202401739.
42. C. Costentin, *Chem. Rev.*, 2008, **108**, 2145-2179.
43. J.-M. Savéant, *Chem. Rev.*, 2008, **108**, 2348-2378.
44. C. Costentin, M. Robert and J.-M. Savéant, *Chem. Rev.*, 2010, **110**, PR1-PR40.

45. K. Sengupta, S. Chatterjee and A. Dey, *ACS Catal.*, 2016, **6**, 6838-6852.
46. C. Costentin and J.-M. Savéant, *Nat. Rev. Chem.*, 2017, **1**, 0087.
47. J.-G. Liu, Y. Shimizu, T. Ohta and Y. Naruta, *J. Am. Chem. Soc.*, 2010, **132**, 3672-3673.
48. Z. Halime, H. Kotani, Y. Li, S. Fukuzumi and K. D. Karlin, *Proc. Natl. Acad. Sci. U. S. A.*, 2011, **108**, 13990-13994.
49. M. T. Kieber-Emmons, M. F. Qayyum, Y. Li, Z. Halime, K. O. Hodgson, B. Hedman, K. D. Karlin and E. I. Solomon, *Angew. Chem. Int. Ed.*, 2012, **51**, 168-172.
50. H. Kim, P. J. Rogler, S. K. Sharma, A. W. Schaefer, E. I. Solomon and K. D. Karlin, *J. Am. Chem. Soc.*, 2020, **142**, 3104-3116.
51. S. Samanta, S. Sengupta, S. Biswas, S. Ghosh, S. Barman and A. Dey, *J. Am. Chem. Soc.*, 2023, **145**, 26477-26486.
52. E. E. Chufán, S. C. Puiu and K. D. Karlin, *Acc. Chem. Res.*, 2007, **40**, 563-572.
53. A. Ray, T. Bristow, C. Whitmore and J. Mosely, *Mass Spectrom. Rev.*, 2018, **37**, 565-579.
54. D. Freitas, X. Chen, H. Cheng, A. Davis, B. Fallon and X. Yan, *ChemPlusChem*, 2021, **86**, 434-445.
55. W. Li, J. Sun, Y. Gao, Y. Zhang, J. Ouyang and N. Na, *Trac-Trends Anal. Chem.*, 2021, **135**, 116180.
56. J. Sun, Y. Yin, W. Li, O. Jin and N. Na, *Mass Spectrom. Rev.*, 2022, **41**, 70-99.
57. X. Zhang, J. Zhan, Z. Yu, J. Deng, M. Li and Y. Shao, *Chin. J. Chem.*, 2023, **41**, 214-224.
58. K. Chen, Q. Wan, S. Wei, W. Nie, S. Zhou and S. Chen, *Chem. Eur. J.*, 2024, **30**, e202402215.
59. L. P. Mark, M. C. Gill, M. Mahut and P. J. Derrick, *Eur. J. Mass Spectrom.*, 2012, **18**, 439-446.
60. D. N. Mortensen and E. R. Williams, *Anal. Chem.*, 2014, **86**, 9315-9321.
61. D. N. Mortensen and E. R. Williams, *J. Am. Chem. Soc.*, 2016, **138**, 3453-3460.
62. R. M. Bain, S. Sathyamoorthi and R. N. Zare, *Angew. Chem. Int. Ed.*, 2017, **56**, 15083-15087.
63. E. T. Jansson, Y.-H. Lai, J. G. Santiago and R. N. Zare, *J. Am. Chem. Soc.*, 2017, **139**, 6851-6854.
64. A. Saha-Shah, J. A. Karty and L. A. Baker, *Analyst*, 2017, **142**, 1512-1518.
65. N. Sahota, D. I. AbuSalim, Melinda L. Wang, C. J. Brown, Z. Zhang, T. J. El-Baba, S. P. Cook and D. E. Clemmer, *Chem. Sci.*, 2019, **10**, 4822-4827.
66. Y. Li, L. Meng, G. Wang, X. Zhou, Z. Ouyang and Z. Nie, *Anal. Chem.*, 2020, **92**, 12049-12054.
67. L. A. Baker and G. S. Jagdale, *Curr. Opin. Electrochem.*, 2019, **13**, 140-146.
68. R. Qiu, X. Zhang, H. Luo and Y. Shao, *Chem. Sci.*, 2016, **7**, 6684-6688.
69. W. Guo, H. Ding, C. Gu, Y. Liu, X. Jiang, B. Su and Y. Shao, *J. Am. Chem. Soc.*, 2018, **140**, 15904-15915.
70. C. Gu, X. Nie, J. Jiang, Z. Chen, Y. Dong, X. Zhang, J. Liu, Z. Yu, Z. Zhu, J. Liu, X. Liu and Y. Shao, *J. Am. Chem. Soc.*, 2019, **141**, 13212-13221.
71. M. Li, P. He, Z. Yu, S. Zhang, C. Gu, X. Nie, Y. Gu, X. Zhang, Z. Zhu and Y. Shao, *Anal. Chem.*, 2021, **93**, 1515-1522.
72. Z. Yu, Y. Shao, L. Ma, C. Liu, C. Gu, J. Liu, P. He, M. Li, Z. Nie, Z. Peng and Y. Shao, *Adv. Mater.*, 2022, **34**, 2106618.
73. X. Zhang, Q.-F. Chen, J. Deng, X. Xu, J. Zhan, H.-Y. Du, Z. Yu, M. Li, M.-T. Zhang and Y. Shao, *J. Am. Chem. Soc.*, 2022, **144**, 17748-17752.
74. Q.-F. Chen, X. Zhang, J. Shi, J. Zhan, F. Xie, H.-T. Zhang, J. Deng, J. Liu, M. Li, Y. Shao and M.-T. Zhang, *CCS Chem.*, 2024, DOI: 10.31635/ccschem.024.202403935.
75. Y. Takahashi, A. I. Shevchuk, P. Novak, Y. Zhang, N. Ebejer, J. V. Macpherson, P. R. Unwin, A. J. Pollard, D. Roy, C. A. Clifford, H. Shiku, T. Matsue, D. Klenerman and Y. E. Korchev, *Angew. Chem. Int. Ed.*, 2011, **50**, 9638-9642.
76. A. Li, A. Hollerbach, Q. Luo and R. G. Cooks, *Angew. Chem. Int. Ed.*, 2015, **54**, 6893-6895.
77. X. Huang and J. T. Groves, *Chem. Rev.*, 2018, **118**, 2491-2553.
78. P. Mondal, I. Ishigami, S.-R. Yeh and G. B. Wijeratne, *Angew. Chem. Int. Ed.*, 2022, **61**, e202211521.

View Article Online
DOI: 10.1039/D5SC00102A

Data availability statements

All experimental data are available in the manuscript and ESI.†